Proceedings of the 12th International Congress on Plasma Physics, 25-29 Oct 2004, Nice (France)

Flux surface shaping effects on tokamak edge turbulence and flows

A. Kendl[1] and B.D. Scott[2]

1) Institut für Theoretische Physik, Universität Innsbruck,
Association EURATOM-ÖAW, A-6020 Innsbruck, Austria.

2) Max-Planck-Institut für Plasmaphysik, EURATOM Association,
D-85748 Garching bei München, Germany.

I. ABSTRACT

The influence of shaping of magnetic flux surfaces in tokamaks on gyrofluid edge turbulence is studied numerically. Magnetic field shaping in tokamaks is mainly due to elongation, triangularity, shift and the presence of a divertor X-point. A series of tokamak configurations with varying elongation $1 \leq \kappa \leq 2$ and triangularity $0 \leq \delta \leq 0.4$, and an actual ASDEX Upgrade divertor configuration are obtained with the equilibrium code HELENA and implemented into the gyrofluid turbulence code GEM. The study finds minimal impact on the zonal flow physics itself, but strong impact on the turbulence and transport.

II. INTRODUCTION

Criteria for a design of future projected magnetized fusion plasma experiments like ITER are primarily based on empirical power laws for the energy confinement time [1]. First-principle based transport models continue as well to require reference to experimental scalings, and are validated mainly only for core plasmas excluding the edge region [2].

The plasma shape of a tokamak enters into confinement time scalings and transport modelling through parameters specifying a vertical elongation $\kappa \geq 1$ and an outboard side triangularity $\delta \geq 0$ that describe the deviation from a simple circular and axisymmetric torus. Scaling laws for plasma confinement are derived by evaluating data from existing tokamaks that usually have only limited possibilities for varying the flux surface shape.

The design criteria of the ITER plasma shape with $\kappa = 1.7$ and $\delta = 0.33$ (at 95% flux surface) are based on a conservative regime that is well established in present experiments [1]. More extreme variations of flux surface shaping were investigated with the experiment TCV (Tokamak à Configuration Variable) which is able to achieve configurations up to $\kappa = 3$ and $\delta = 0.5$ [3]. Experimental evidence suggests that large elongation is always

beneficial for local and global energy confinement, whereas the effect of triangularity is smaller and can even change sign depending on the size of the Shafranov shift.

One of the main requirements for successful performance of future fusion experiments is the prospect of operation in a high confinement H-mode. The formation of a transport barrier in a magnetically confined toroidal H-mode plasmas is closely related to the presence of radially sheared poloidal or toroidal flows which act to suppress turbulent convection [4,5]. Both neoclassical particle dynamics and also zonal structures in turbulent potential fluctuations can lead to radially varying electric fields $\tilde{\mathbf{E}}(r)$ that drive flows with velocity $\mathbf{v}_E = (c/B^2)\tilde{\mathbf{E}} \times \mathbf{B}$ perpendicular to a background magnetic field $\mathbf{B}$ [6–8].

The transition between states of low plasma confinement (L-mode) to the high confinement regime featuring such an edge transport barrier (H-mode) is up to now not satisfactorily described by any of the existing first-principle theories [9]. The notion that generation of zonal flows by inverse cascade of the turbulence can act to self-regulate by suppressing the driving turbulent vortices has lead to the development of predator-prey type bifurcation models that are able to describe specific characteristics of the L-H transition (see e.g. [10]). Early computations based on the resistive-g [11] and collisional drift wave [12] models found self-generated sheared flows which could be argued as an L-H transition trigger. However, more recent models in more comprehensive treatment of the toroidal geometry do not find this [13].

After the initial discovery in the early divertor experiment ASDEX [14] it has been found in numerous large tokamaks around the world that the presence of a divertor (originally designed to improve the impurity exhaust) significantly enhances the prospect of reaching the H-mode state.

There have been several approaches to model the confinement transition in magnetized plasmas [9]. Validation of such models by numerical simulation and improved theory is an issue of outstanding importance. Up to now both the transition models as well as the numerical simulations have relied mainly on much oversimplified representations of the plasma geometry. In our present work we intend to test the foundations of confinement and transition models by using basic first-principle numerical simulations of plasma turbulence that implement realistic flux surface shaping effects into a gyrofluid tokamak edge code. The aim is to test and in principle falsify particular theoretical bases for heuristic models and scenarios which are then applied to experimental modelling.

Spin-up and suppress scenarios (self generated zonal flows whose return effect should be to reduce the turbulence and transport)in transition models can qualitatively be reproduced by first-principle simulations of edge turbulence [11,12]. However, the introduction of 3D toroidal compressibility of the zonal flows opens channels in the nonlinear dynamics of the vortex-flow interaction that strongly affect the flow energetics [16,17]. The ori-

gin of the compression is the geodesic curvature of the magnetic field lines. The flow is thereby coupled with poloidally asymmetric pressure sidebands which are consumed by the turbulence and global Alfvén or parallel flow dynamics. This geodesic transfer mechanism represents a restoring loss channel for the zonal flows, ultimately placing them in statistical equilibrium with the turbulence, with the Reynolds stress (spin-up) mechanism continuing to operate. Since the latter acts on all frequencies, the geodesic acoustic mode (GAM) oscillation itself need not be present for the geodesic transfer mechanism to operate. The net result of this is that turbulent transport in 3D toroidal edge computations is found to be reduced but not completely suppressed by the self-generated zonal flows.

This geodesic transfer effect was first studied for the case of a basic circular toroidal magnetic field. Modern tokamak plasma experiments exhibit a shaping of the confining magnetic field that is considerably different from a perfect torus and feature characteristics like a quasi elliptic elongation in the horizontal direction of up to a factor 2, some triangularity on the outboard field side, and are usually equipped with a divertor for impurity exhaust that introduces an X-point in the magnetic field. Field lines are accordingly strongly and inhomogenously sheared and curved in the closed flux surface region of the plasma edge near the separatrix. A schematic view of a shaped plasma cross section is shown in Fig. 1.

In the following we give both first-principle numerical evidence and a clear physical picture of how plasma shaping and the presence of a divertor via its modification of plasma geometry can influence the outcome of the turbulence/flow interaction.

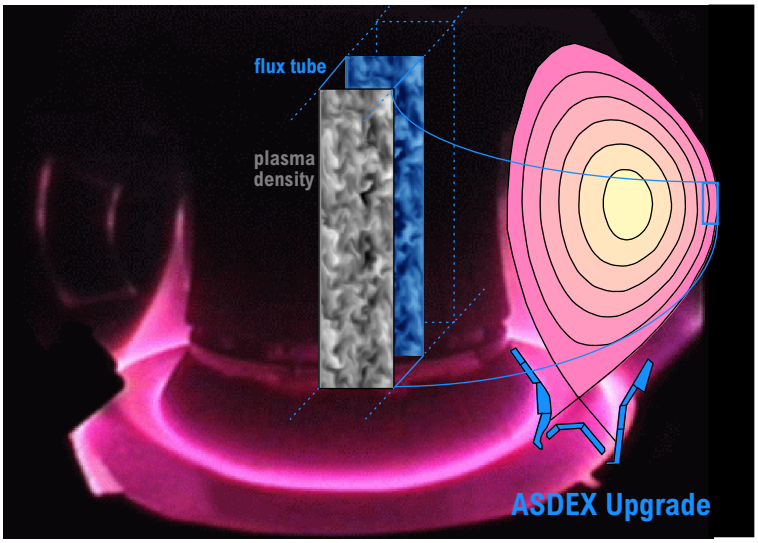

FIG. 1. Poloidal cross section of a tokamak plasma (ASDEX Upgrade) showing the elongation and triangularity of closed flux surfaces and a lower X-point on the separatrix. A section of the flux tube for drift wave turbulence simulations winding around the torus along field lines is here locally intersecting the outer midplane of the plasma edge.

III. THE GYROFLUID ELECTROMAGNETIC MODEL GEM3

Transport in a fusion edge plasma is dominated by turbulent low-frequency drift wave motion that causes a fluid-like convection through $E \times B$ vortices in a plane perpendicular to the magnetic field direction.

The gyrofluid electromagnetic two-moment model GEM3 is a generalisation of the drift-Alfvén wave equations for describing tokamak edge turbulence in the isothermal approximation. By constructing moments from the nonlinear gyrokinetic equation the gyrofluid continuity equations for the perturbed densities $\tilde{n}_i$ and $\tilde{n}_e$ and the force balance equations for the parallel velocities $\tilde{u}_\parallel$ and $\tilde{v}_\parallel$ can be obtained. The tilde symbol denotes dependent variables, disturbances on a background which is homogeneous except for density profile gradients given by ∇n_{i0} and ∇n_{e0}, with scale length given by the additional parameter $L_\perp$ (for additional details cf. Ref. [18] for the equations and parameters and Ref. [21] for the geometry). The ion equations are:

$$\frac{1}{n_i}\left(\frac{\partial}{\partial t} + \mathbf{u}_E \cdot \nabla\right)(\tilde{n}_i + n_{i0}) = -B\nabla_\parallel \frac{\tilde{u}_\parallel}{B} + \mathcal{K}\left(\tilde{\phi}_G\right) + \frac{T_i}{n_i e}\mathcal{K}\left(\tilde{n}_i\right) \tag{1}$$

$$\frac{1}{c}\frac{\partial \tilde{A}_\parallel}{\partial t} + \frac{M_i}{e}\left(\frac{\partial}{\partial t} + \mathbf{u}_E \cdot \nabla\right)\tilde{u}_\parallel = -\nabla_\parallel \tilde{\phi}_G - \frac{T_i}{n_i e}\nabla_\parallel\left(\tilde{n}_i + n_{i0}\right) - \eta_\parallel \tilde{J}_\parallel \tag{2}$$

and the electron equations are

$$\frac{1}{n_e}\left(\frac{\partial}{\partial t} + \mathbf{v}_E \cdot \nabla\right)(\tilde{n}_e + n_{e0}) = -B\nabla_\parallel \frac{\tilde{v}_\parallel}{B} + \mathcal{K}\left(\tilde{\phi}\right) - \frac{T_e}{n_e e}\mathcal{K}\left(\tilde{n}_e\right) \tag{3}$$

$$\frac{1}{c}\frac{\partial \tilde{A}_\parallel}{\partial t} - \frac{m_e}{e}\left(\frac{\partial}{\partial t} + \mathbf{v}_E \cdot \nabla\right)\tilde{v}_\parallel = -\nabla_\parallel \tilde{\phi} + \frac{T_e}{n_e e}\nabla_\parallel\left(\tilde{n}_e + n_{e0}\right) - \eta_\parallel \tilde{J}_\parallel \tag{4}$$

with the current given by

$$\frac{4\tilde{\pi}}{c}J_\parallel = n_i e\tilde{u}_\parallel - n_e e\tilde{v}_\parallel = -\nabla_\perp^2 \tilde{A}_\parallel. \tag{5}$$

The two species are in addition connected by gyrofluid polarisation,

$$\Gamma_1 \tilde{n}_i e + n_i e^2 \frac{\Gamma_0 - 1}{T_i}\tilde{\phi} = \tilde{n}_e e, \qquad \text{with } \Gamma_0 \text{ approximated by } \Gamma_0 = (1 - \rho_i^2 \nabla_\perp^2)^{-1}. \tag{6}$$

The operator Γ_0 gives the averaging to express guiding centre densities in terms of space densities.

Finite gyroradius effects for electrons are neglected, but the ions are subjected to the reduced potential $\tilde{\phi}_G$ given by weighted gyroaveraging,

$$\tilde{\phi}_G = \Gamma_1(\tilde{\phi}), \qquad \text{with } \Gamma_1 = \Gamma_0^{1/2}, \text{ approximated by } \Gamma_1 = (1 - \frac{1}{2}\rho_i^2 \nabla_\perp^2)^{-1}. \tag{7}$$

The $E \times B$ advection velocity for electrons is $\mathbf{v}_E = (c/B^2)\mathbf{B} \times \nabla\phi$, and the finite gyroradius equivalent for ions is $\mathbf{u}_E = (c/B^2)\mathbf{B} \times \nabla\phi_G$.

The differential operators are the parallel gradient

$$\nabla_\parallel = (1/B)(\mathbf{B} + \tilde{\mathbf{B}}_\perp) \cdot \nabla, \tag{8}$$

with magnetic field disturbances $\tilde{\mathbf{B}}_\perp = (-1/B)\mathbf{B} \times \nabla\tilde{A}_\parallel$ as additional nonlinearities, the perpendicular Laplacian

$$\nabla_\perp^2 = \nabla \cdot [(-1/B^2)\mathbf{B} \times (\mathbf{B} \times \nabla)], \tag{9}$$

and the curvature operator

$$\mathcal{K} = \nabla \cdot [(c/B^2)\mathbf{B} \times \nabla)]. \tag{10}$$

The edge plasma is further characterised by collisionality $C = 0.51\hat{\epsilon}(\nu_e c_s/L_\perp)(m_e/M_i)$, magnetic induction $\hat{\beta} = \hat{\epsilon}(4\pi p_e/B^2)$, electron inertia $\hat{\mu} = \hat{\epsilon}(m_e/M_i)$ with the scale ratio parameter controlling the ion inertia, $\hat{\epsilon} = (qR/L_\perp)^2$, and $c_s = \sqrt{T_e/M_i}$ is the sound speed. We choose nominal parameters to reflect typical tokamak edge conditions: $C = 5, \hat{\beta} = 1, \hat{\mu} = 5$ and $\hat{\epsilon} = 18350$.

The computational domain is set to 64×256 nodes in units of the drift scale $\rho_s = (c/eB)\sqrt{T_e M_i}$ for (x, y) and 16 nodes in one field line connection length $(2\pi qR)$ in $-\pi < z < \pi$. The dimensions are chosen to appropriately account for statistical isotropy in small scales in both perpendicular directions with satisfactory spectral overlap, and for an extended box size in the electron drift direction y to reflect the "thin-atmosphere" nature of the edge layer. A grid resolution down to ρ_s together with a radial (x) domain size comparable to $L_\perp$ guarantees inclusion of all scales necessary for the nonlinear dynamics that are essential for the drift wave turbulence characteristics [16].

IV. FLUX TUBE REPRESENTATION OF TOKAMAK GEOMETRY

Tokamak equilibria are computed by solving the Grad-Shafranov / Lüst-Schlüter equation with the code HELENA [20], implemented as described in Ref. [13]. A set of nested flux surfaces in straight field line Hamada coordinates (V, θ, ζ) is obtained by specification of given radial profiles of pressure and rotational transform, and of the shape of the bounding last closed flux surface. These Hamada coordinates are then transformed into a field aligned system and re-scaled into local flux tube coordinates (x, y, z) [19].

A transformation of the coordinate y, which signifies the electron diamagnetic drift direction perpendicular to the magnetic field within flux surfaces, is applied in order to avoid grid deformation by local magnetic shear [21] .Otherwise, grid cells are sheared strongly in y direction particularly near the X-point region, with malign consequences on

nonlinear dynamics, especially in the vorticity, that lead to a violation of the basic drift wave character and overestimate linear MHD-like dynamics. The differential operators are then expressed in terms of the flux tube coordinates: The curvature operator becomes

$$\mathcal{K} = \mathcal{K}^x(z)\nabla_x + \mathcal{K}^y(z)\nabla_y, \tag{11}$$

the perpendicular Laplacian in flute mode ordering is

$$\nabla_\perp^2 = g^{xx}(z)\frac{\partial^2}{\partial x^2} + 2g^{xy}(z)\frac{\partial^2}{\partial x \partial y} + g^{yy}(z)\frac{\partial^2}{\partial y^2}, \tag{12}$$

and the parallel derivative is

$$\nabla_\parallel = b^z(z)\frac{\partial}{\partial z}, \tag{13}$$

noting also that the factor of B^2 in ρ_i^2 also depends on z. Some metric coefficients g^{ij} that were obtained for elongation $\kappa = 1$ and $\kappa = 2$ with triangularity $\delta = 0$ and $\delta = 0.4$ are shown in Fig. 2. Increasing elongation κ specifically rises the local magnetic shear $S = \nabla_\parallel(g^{xy}/g^{xx})$ and reduces $\mathcal{K}^x$ both in the upper and lower regions of the torus that correspond to flux tube coordinates $z = \pm\pi/2$. Local and global magnetic shear have a damping influence on tokamak edge turbulence [15], whereas geodesic curvature acting through $\mathcal{K}^x$ upon $k_y = 0$ modes maintains the coupling for a loss channel from zonal flow energy eventually to turbulent vortices [16]. Both mechanisms help to reduce the local turbulent $E \times B$ heat transport $\mathbf{Q} = T\langle \mathbf{v}_{E\times B}\tilde{n}\rangle$. Normal curvature $\mathcal{K}^y$ on the other hand strengthens primarily the interchange forcing of the turbulence ($k_y \neq 0$).

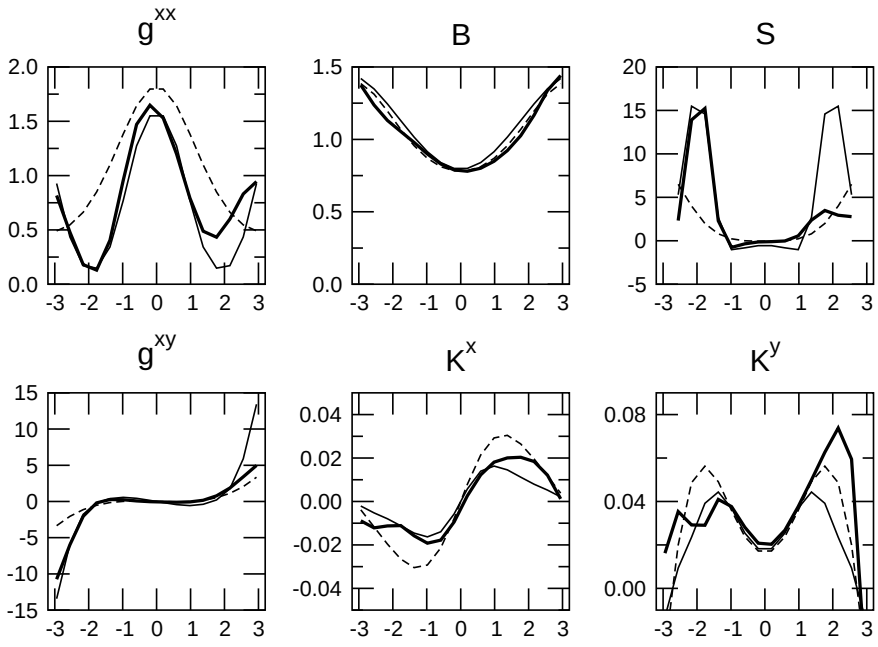

FIG. 2. Metric element g^{xx}, g^{xy} (unshifted), normal curvature $\mathcal{K}^y$, geodesic curvature $\mathcal{K}^x$, magnetic field strength B and local magnetic shear S in a tokamak with elongation $\kappa = 1$ and triangularity $\delta = 0$ (dashed lines), compared to a configuration with $\kappa = 2$ and $\delta = 0.4$ (thin solid lines) and to an actual ASDEX Upgrade configuration (bold solid lines).

V. INFLUENCE OF ELONGATION AND TRIANGULARITY ON TURBULENCE AND TRANSPORT

We construct a series of tokamak equilibria for elongation $\kappa = 1.00, 1.25, 1.50, 1.75, 2.00$ and triangularity $\delta = 0, 0.1, 0.2, 0.3$ and 0.4 with equal profiles of pressure and rotational transform. The flux tube is chosen for a radial position $V/V_0 = 0.90$ which for typical L-mode tokamak experiments is located in the strong pressure gradient pedestal region defining the plasma edge. The background density profile and rotational transform are linearised within the bounds of the radial computational domain. We restrict our simulations for now to the closed field line region lying a few tens of ion gyroradii inside from the separatrix, thus avoiding complications that occur by a divergent metric and associated grid deformation when the last closed flux surface is approached in the vicinity of an X-point. Ultimately, the goal of edge turbulence simulations will be to combine sufficiently well resolved nonlocal drift wave computations with a representation of the realistic field line geometry crossing the separatrix to the bounded scrape-off layer region.

When the plasma shape is thus varied, we have a particular interest in the effects on fluctuation time and spatial scales, on the radial variation of flux surface averaged (zonal) flows, and on turbulent transport.

The cross-field turbulent transport is locally determined by the radial component of $E \times B$ convection of the fluctuating density and thus for isothermal plasma given by

$$Q_e = T_e \tilde{v}_x \tilde{n}_e \quad \text{and} \quad Q_i = T_i \tilde{u}_x \tilde{n}_i. \tag{14}$$

The local flows $Q(x, y, z)$ are fluctuating in time, and for specifying a quantitative value to it the time average over a sufficiently long window, that covers all relevant frequency scales, is taken during the final phase of simulations after all initial linear transients and spin-up of flows and oscillations have reached saturation. The zonally averaged (over the yz-domain) flux is given by $\langle Q(x) \rangle_{y,z}$. The units of transport fluxes obtained by this procedure are given by standard gyro-Bohm normalisation to $p_e c_s (\rho_s / L_\perp)^2$. The integration obtaining the global transport across an entire magnetic flux surface takes the variation of surface area with elongation into account: the poloidal circumference λ of an ellipse scales roughly like $\lambda \approx 2\pi r[0.75(1+\kappa^2)/\kappa - 0.5]$ which gives $\lambda(\kappa \equiv 2) \approx 1.4\lambda(\kappa \equiv 1)$ for volume-averaged flux surface radius $r = \sqrt{V/2\pi R_0}$. We observe that the influence of elongation via the turbulence dynamics on local transport fluxes is much larger than the additional factor on global scalings given by this surface factor: The electron transport flux F_e (where $Q_e = T_e F_e$) shown in Fig. 3 is reduced to more than a third when elongation is increased from a circular cross section to $\kappa = 2$.

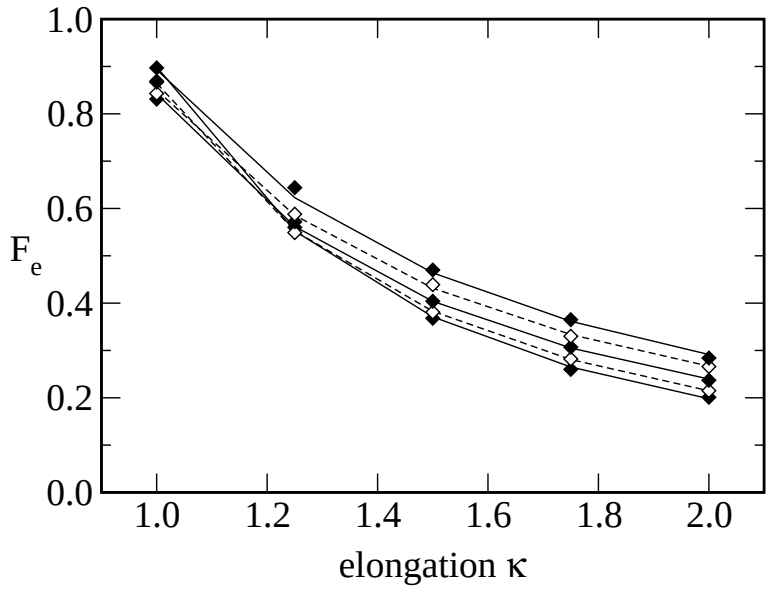

FIG. 3. Dependence of turbulent electron transport F_e (in gyro-Bohm units) on elongation κ for various values of triangularity between $\delta = 0$ and 0.4.

The same set of data results for F_e is displayed against triangularity δ in Fig. 4. For $\kappa = 1$ the transport flux is independent from triangularity within the error bars given by the deviation of the fluctuating data from its time average. For higher elongation $\kappa = 2$ we observe that transport F_e is increased from the normalised value of 0.20 to 0.28 by increasing triangularity from 0 to 0.4.

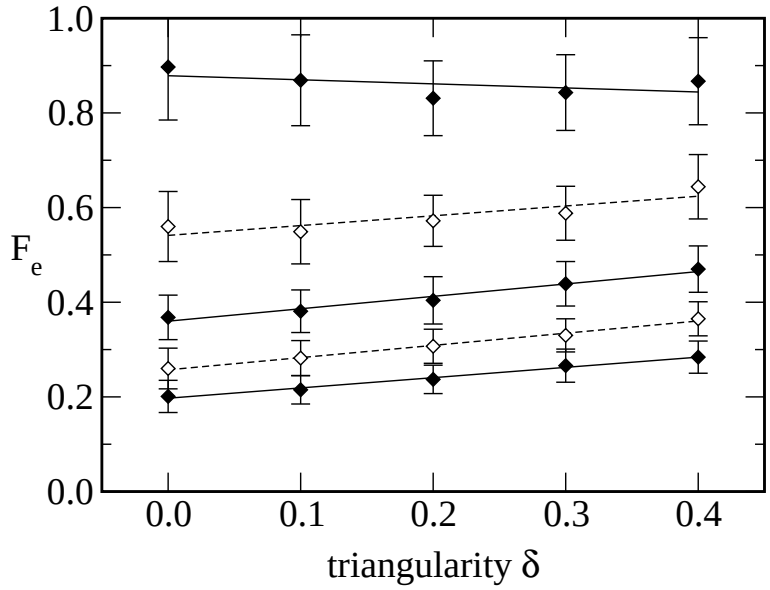

FIG. 4. Same data as Fig. 3: Dependence of turbulent transport F_e on triangularity δ for various values of elongation between $\kappa = 1$ (top) and 2 (bottom). Error bars show the standard deviation of fluctuating data from their time average.

A good fit to the transport data within fluctuation error bars is obtained by

$$F_e(\kappa, \delta) \approx F_{1,0} \cdot \kappa^{-2.15+1.46\delta} \tag{15}$$

where $F_{1,0} = F(\kappa = 1, \delta = 0)$. For fixed gradients and in the present isothermal approximation, the local diffusivity χ is proportional to F_e and thus to the roughly inverse quadratic scaling with κ given in Eq. 15. At a glance, this appears to contradict the naive view one may find by simply deconstructing global experimental energy confinement scalings, which can lead to inferring a nearly complete lack of κ scaling on local transport [22]. The latter result was obtained by assuming a scaling of χ with a safety factor $q(\kappa)$: there, a variation of q with elongation is a result of the assumption of independently scaling toroidal current I and toroidal magnetic field B_T. In addition, the thermal energy content of the plasma is approximated by the average pressure and total volume V, where $V \sim \kappa$ has been assumed. This assumption might be too crude, as flux surfaces are more circular towards the plasma centre where the pressure is largest, than at the edge at which κ usually is defined.

In our computations, however, the same q and p profiles are maintained in the calculation of the numerical equilibria throughout variations of κ and δ in HELENA. This approach is favourable when the attention shall be focused on first principle physics mechanisms, like the geodesic transfer effect and normal curvature forcing in our present study. The complimentary approach to calculate the equilibria by specifying $I(r)$ instead of $q(r)$ will lead to a rise of both q and global magnetic shear $\hat{s} = (r/q)(\partial q/\partial r)$ with increasing elongation. While stronger shear reduces the turbulent transport [15], an increase in q enters into the parallel to perpendicular scale length ratio $\epsilon = (qR/L_\perp)^2$, which directly scales fundamental plasma parameters ($\hat{\mu}$, $\hat{\beta}$) and the coupling of curvature operators in the turbulence code. It will of course be worthwhile to undertake such a complimentary approach in some future turbulence study in order to validate the empirical scaling.

VI. SHEARED FLOWS IN THE PRESENCE OF A TOKAMAK DIVERTOR

Time traces are resolved down to 1/20th of the drift frequency $\omega_{DW} = c_s/L_\perp$, and long computational runs are required to account for zonal flows with $\omega \approx 0$. A typical number of time steps is 10^5. Geodesic acoustic mode (GAM) oscillations may be distinctly detectable for some parameters and are expected for circular geometry around $\omega/\omega_{DW} = (2L_\perp/R)\sqrt{(1+\tau_i)/2}$. In our case, $\omega_{GAM} = 0.03\omega_{DW}$. In general, the GAM frequency is determined by the geodesic curvature term $\mathcal{K}^x$ and is influenced by flux surface deformation.

The variation of $\mathcal{K}^x$ with elongation κ in the HELENA metric can be understood by expressing the cylindrical coordinates (R, Φ, Z) of a plasma in an axisymmetric configurations in terms of flux coordinates (ρ, θ, ϕ) by

$$R = R_0 + (\rho/\kappa)\cos\theta \quad \text{and} \quad Z = (\rho\kappa)\sin\theta. \tag{16}$$

The geodesic curvature effect is the action of the curvature operator $\mathcal{K}$ upon $k_y = 0$. In local flux tube coordinates and low beta approximation this works through the part

$$\mathcal{K}^x \partial_x = (cB_0/B^2)(\partial_z \ln B^2)\partial_x \tag{17}$$

where the radial dependence of the magnetic field strength may in a low aspect ratio approximation ($\epsilon = \rho/R_0 \ll 1$) be written as

$$B \approx B_0 R_0/R = B_0[1 + (\epsilon/\kappa)\cos\theta]^{-1}, \tag{18}$$

where in flux tube coordinates $z = \theta$, so that

$$\mathcal{K}^x \sim \left(\frac{2\rho}{R}\right)\frac{1}{\kappa}\sin\theta. \tag{19}$$

This factor $1/\kappa$ in the geodesic curvature term does also accordingly scale the geodesic acoustic mode frequency: stronger elongation shifts the GAM resonance frequency in the spectrum closer to the zero-frequency zonal flow. The same argument, now applied to the normal curvature term $\mathcal{K}^y$, also accounts for a corresponding scaling of the (interchange) drift wave frequency likewise with κ^{-1}.

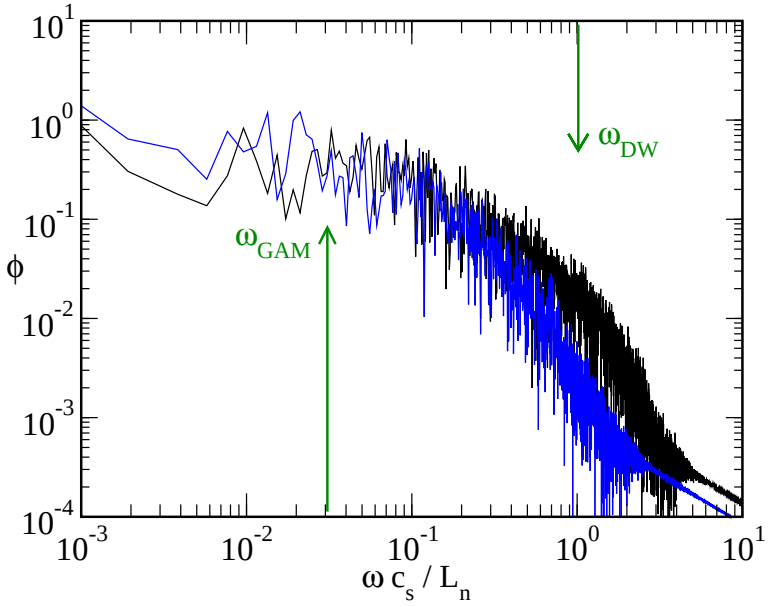

FIG. 5. Local frequency spectra $\tilde{\phi}(\omega)$ for $\kappa = 1$ (black) and $\kappa = 2$ (blue), both for $\delta = 0$. Arrows indicate the drift wave and GAM resonances.

For the parameters used in our computations, the GAM peak does not protrude very distinctly but can still be identified on the flat top of the spectra. In Fig. 5 the discrete Fourier transform spectrum $\tilde{\phi}(\omega)$ for a measurement of $\tilde{\phi}$ at a local point in the centre of the xyz-domain is shown: the spectrum below the GAM resonance is mostly flat except

for the distinct zonal flow peak at $\omega = 0$. The higher frequency part shows a typical $\omega^{-\alpha}$ cascade structure, where the exponent α changes at some point for larger frequencies. The change of exponent occurs around the drift frequency $\hat{\omega} \approx 1$, which for our choice of edge parameters coincides also with the Alfvén frequency. One may identify three ranges in the spectrum: A flat top region between the zonal flows and GAM frequencies, one intermediate cascade range between the GAM and drift wave frequencies with $\alpha \approx 1 - 2$, and another cascade range between the drift wave and the dissipation times scale with $\alpha \approx 3 - 5$.

As expected from the above considerations, both GAM and drift wave frequencies are reduced by increasing elongation to lower values $\omega \to \omega/\kappa$. The whole spectrum is thus shifted to the left for $\kappa = 2$ in Fig. 5.

In addition to computing the flux surface shapes with varying elongation and triangularity discussed above, HELENA can also be used to obtain equilibria with an outer boundary defined by an experimentally reconstructed separatrix position. In this way we obtain an equilibrium in the typical shape of an ASDEX Upgrade (AUG) [23] lower single null divertor configuration (as shown in Fig. 1). The additional asymmetric shaping by the presence of an X-point in the lower part of the torus leads to an increase of local magnetic shear near $z = -\pi/2$ and an associated local reduction of geodesic curvature. The elongation and triangularity of this configuration are otherwise comparable to $\kappa \approx 1.6$ and $\delta = 0.3$. This AUG configuration was first used in edge turbulence computations in Ref. [19], where the dependence of transport on $\hat{\beta}$, and thus on the Shafranov pressure shift, was established: it was found that the onset of MHD ballooning mode turbulence is prevented for typical tokamak edge parameters due to the shaping effects in realistic geometry, and the nature of transport is still basically of the drift-Alfvén wave character.

The local magnetic shear $S = \partial_z g^{xy}/g^{xx}$ is displayed in Fig. 2 for the AUG model, the circular $\kappa = 1$ and the elongated tokamak $\kappa = 2$. For the upper region of the torus near $z = +\pi/2$ the local shear is comparable to the case of an equivalent up-down symmetric configuration with the average elongation $\kappa_{AUG} = 1.6$. In the lower part around $z = -\pi/2$ near the X-point we see that S is increased to a level corresponding to an elongation of 2. On flux surfaces nearer to the separatrix ($V/V_0 = 1$) than the present radius ($V/V_0 = 0.90$) local magnetic shear is further considerably increased in the X-point region, whereas geodesic curvature $\mathcal{K}^x$ is further lowered. The AUG model thus has, for the present flux tube position, properties relevant to the turbulence dynamics that are in some aspects in between those of up-down symmetric configurations with $\kappa = 1.6$ and 2.0. Transport in the AUG model is reduced to $F_e = 0.5$ compared to $F_e = 0.9$ for the circular torus. The nonlinear growth rate $\Gamma_N = F_e/2E_{tot}$ is only slightly lower for the AUG model with $\Gamma_N = 0.007 \pm 0.001$ than for the circular torus with $\Gamma_N = 0.0085 \pm 0.001$.

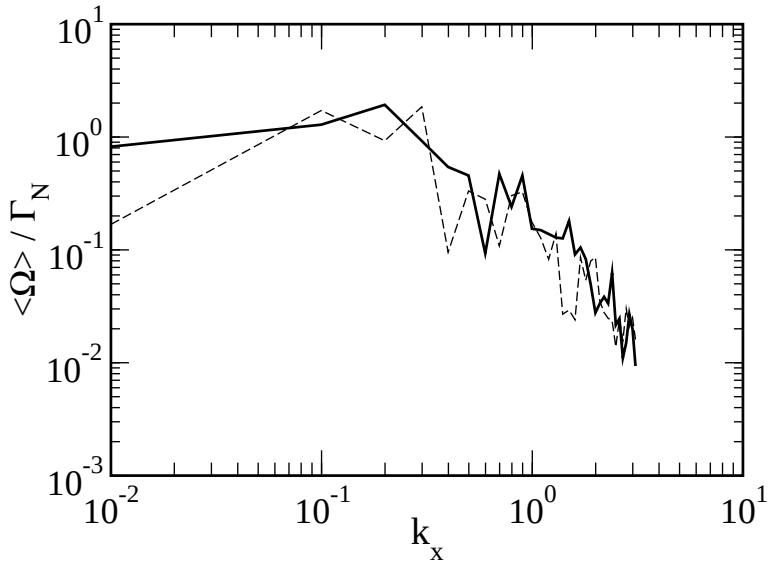

FIG. 6. Radial k_x spectra of flux surface averaged vorticity $\langle\Omega\rangle = \partial_x\langle u_y\rangle$, related to nonlinear growth rate Γ_N: the ASDEX Upgrade configuration (bold line) has slightly larger (+16 %) cumulative amplitude in all modes of the vorticity spectrum than the circular tokamak (thin dashed line). The reduction of geodesic curvature with increasing κ thus enhances the shear flow only insignificantly by effectively lowering the coupling of zonal flows to GAMs.

A reduction of geodesic curvature by elongation and X-point shaping might be expected to lead to a weakening of the geodesic transfer coupling mechanism for energy from zonal flows to GAMs. This can be analysed by comparing the flux surface averaged vorticity

$$\langle\Omega(x)\rangle = \partial_x\langle u_y(x)\rangle \tag{20}$$

for the configurations of the circular torus with the AUG model. The zonal flow velocity $u_y(x)$ is derived from the electrostatic potential fluctuations by $\langle u_y(x)\rangle = (c/B)\partial_x\langle\tilde{\phi}(x)\rangle$. The zonal vorticity $\langle\Omega\rangle$ thus represents the radial shearing of zonal flows, which is considered responsible for the turbulent shear flow decorrelation and energetic damping of vortices [10]. Concerning the geometric effect on this, however, we find that the cumulative amplitude of the modes in the radial spectrum of zonal vorticity is only slightly increased by $10-20\%$ for the elongated AUG for $\langle\Omega\rangle$ expressed in terms of the nonlinear growth rate Γ_N in Fig. 6. The lowest k_x mode in these spectra makes up for approximately 8% of the total vorticity. Evidence for an enhancement of shear flows by elongation and X-point shaping is present but weak. The reduction of turbulent edge transport is thus mainly a result of the local magnetic shear effect [15].

It can be expected that the enhancement of zonal flows is more pronounced for stronger shaping, when the separatrix is approached by either specifying a flux tube nearer to $V/V_0 = 1$, or by allowing for a radially inhomogeneous metric in the turbulence code in simulations with global profile evolution. We have observed in such global models that a spin-up of zonal flows in a radially narrow region of the computational domain

(e.g. by injecting vorticity locally) can extend to broader parts of the x-domain. A realistic representation of the geometry approaching the X-point however requires high grid resolution and is computationally challenging even for a code like GEM3 which applies coordinate techniques designed to mitigate this problem.

VII. CONCLUSION

We have presented results for simulations of gyrofluid edge turbulence in realistic tokamak geometry. It is found that turbulent transport F_e is reduced by increasing flux surface elongation κ. The influence of triangularity δ is much weaker and generally also depends on elongation and on a pressure shift. While geodesic acoustic modes (GAM) and the overall turbulence frequency spectra depend on flux surface geometry, we find only a minor enhancement of flow shear by elongation and X-point shaping. The damping of transport observed in our simulations in realistic tokamak geometry is mainly a result of local magnetic shear.

---

[1] V. Mukhovatov *et al.*, Plasma Phys. Contr. Fusion **45**, A235 (2003).
[2] A.M. Dimits *et al.*, Phys. Plasmas **7**, 969 (2000).
[3] J.M. Moret *et al.*, Phys. Rev. Lett. **79**, 2057 (1997).
[4] K.H. Burrell, Phys. Plasmas **4**, 1499 (1997).
[5] P. W. Terry, Rev. Mod. Phys. **72** 109 (2000).
[6] R.J. Groebner, K.H. Burrell, and R.P. Seraydarian, Phys. Rev. Lett. **64**, 3015 (1990).
[7] J.A. Heikinnen, T.P. Kiviniemi, and A.G. Peeters, Phys. Rev. Lett. **84** 487 (2000).
[8] M.G. Shats, W.M. Solomon, and H. Xia. Phys. Rev. Lett. **90**, 125002 (2003).
[9] J.W. Connor and H.R. Wilson, Plasma Phys. Control. Fusion **42**, R1 (2000).
[10] P.H. Diamond, Y.M. Liang, B.A. Carreras, and P.W. Terry, Phys. Rev. Lett. **72**, 2565 (1994).
[11] B.A. Carreras, V.E. Lynch, L. Garcia, and P.H. Diamond, Phys. Fluids B **5**, 1491 (1993).
[12] B.D. Scott, in *Plasma Phys. and Contr. Nuclear Fusion Research 1994*, IAEA Vienna 1996, Vol. 3, p. 447.
[13] B.D. Scott, Phys. Plasmas **7**, 1845 (2000).
[14] F. Wagner *et al.*, Phys. Rev. Lett. **49**, 1408 (1982).
[15] A. Kendl and B.D. Scott, Phys. Rev. Lett. **90**, 035006 (2003).
[16] B.D. Scott, Phys. Letters A **320**, 53 (2003).
[17] H. Hallatschek and D. Biskamp, Phys. Rev. Lett. **86**, 1223 (2001).
[18] B.D. Scott, Plasma Phys. Contr. Fusion **45**, A385 (2003).
[19] B.D. Scott, Phys. Plasmas **5**, 2334 (1998).
[20] G.T.A. Huysmans, J.P. Goedbloed and W. Kerner, Proc. CP90 Conf. on Comp. Phys, World Scientific Publ. Co, 371 (1991).
[21] B.D. Scott, Phys. Plasmas **8**, 447 (2001)
[22] G. Becker, Nucl. Fusion **42**, L8 (2002).
[23] A. Herrmann (ed.) Fusion Science and Technology **44** (Special Edition), 569 (2003)